



Structural Damage Assessment of a Five Tiered Pagoda Style Temple in Nepal

Richard L. Wood⁽¹⁾, Mohammad Ebrahim Mohammadi⁽²⁾, Andre R. Barbosa⁽³⁾ Chandra Kiran Kawan⁽⁴⁾,
Manjip Shakya⁽⁵⁾, Michael J. Olsen⁽⁶⁾

⁽¹⁾ Assistant Professor, Department of Civil Engineering, University of Nebraska-Lincoln, Lincoln NE, USA, rwood@unl.edu

⁽²⁾ Graduate Student, Department of Civil Engineering, University of Nebraska-Lincoln, Lincoln NE, USA, mmohammadi2@unl.edu

⁽³⁾ Assistant Professor, School of Civil & Construction Engineering, Oregon State University, Corvallis, OR, USA,
andre.barbosa@oregonstate.edu

⁽⁴⁾ Associate Professor, Department of Civil Engineering, Khwopa College of Engineering, Bhaktapur,
Nepal, kawan.chandra1@gmail.com

⁽⁵⁾ Senior Lecturer, Department of Civil Engineering, Khwopa Engineering College, Bhaktapur, Nepal, maanzeep@gmail.com

⁽⁶⁾ Associate Professor, School of Civil & Construction Engineering, Oregon State University, Corvallis, OR, USA,
michael.olsen@oregonstate.edu

Abstract

The April 2015 M7.8 Gorkha Earthquake and its aftershocks caused extensive damage to numerous cultural heritage sites throughout Nepal. While many structures experienced complete collapses, one of the most recognizable cultural heritage sites that suffered damage was the five-tiered Nyatapola Temple, a UNESCO World Heritage site located in Bhaktapur, Nepal. This temple was originally completed in 1702 and survived both the 1934 Nepal-Bihar and 2015 Gorkha Earthquake and subsequent aftershocks. However, this historical temple experienced extensive cracks within the unreinforced masonry brick walls with mud-mortar during the 2015 earthquake. As a result, the authors collected detailed assessment data to characterize its state in the aftermath of the 2015 earthquake to inform potential rehabilitation solutions.

The data collected includes ambient vibration data and ground-based lidar. The ambient vibration data was collected via accelerometers placed each roof level in three different setups. Twenty-four minutes of data for each setup were obtained to identify the modal parameters using output-only system identification techniques. To complement the ambient vibration data, over 35 lidar scans were performed over two days to quantify the extent of cracking on the exterior and interior walls. Both of these sensing techniques provide important information for the development of an initial finite element model. The developed finite element model aids in the understanding of the response of this structure and give insight to the performance of this and other historical Pagoda style temples in future earthquake events.

Keywords: Lidar; System Identification; Damage Detection; 2015 Gorkha Earthquake; Remote Sensing.

1 Introduction

The M_w 7.8 Gorkha earthquake occurred on Saturday, April 25, 2015, at 11:41 A.M. local time within the Gorkha district of central Nepal (28.15° N, 84.70° E) with a focal depth of 15 km. Various levels of ground shaking were felt throughout Nepal, as well as regions of India, Bhutan, Bangladesh, Tibet, and China (Fig. 1b). Within a few days of the main seismic event, significant aftershocks of M_w 6.6 and 6.7 occurred, as well as one particularly strong aftershock of M_w 7.4 on May 12, 2015, located approximately 80 km northeast of Kathmandu [1]. The main shock of the earthquake was noted to have a moderate peak ground acceleration of 0.25 g on hard rock southwest of the capital city of Kathmandu; however, basin effects were observed throughout the Kathmandu Valley. One station approximately 7 km east of downtown Kathmandu, on slightly consolidated soil, has a reduced peak ground acceleration; however, a significant pulse occurs in the long period as illustrated in Fig. 1b.

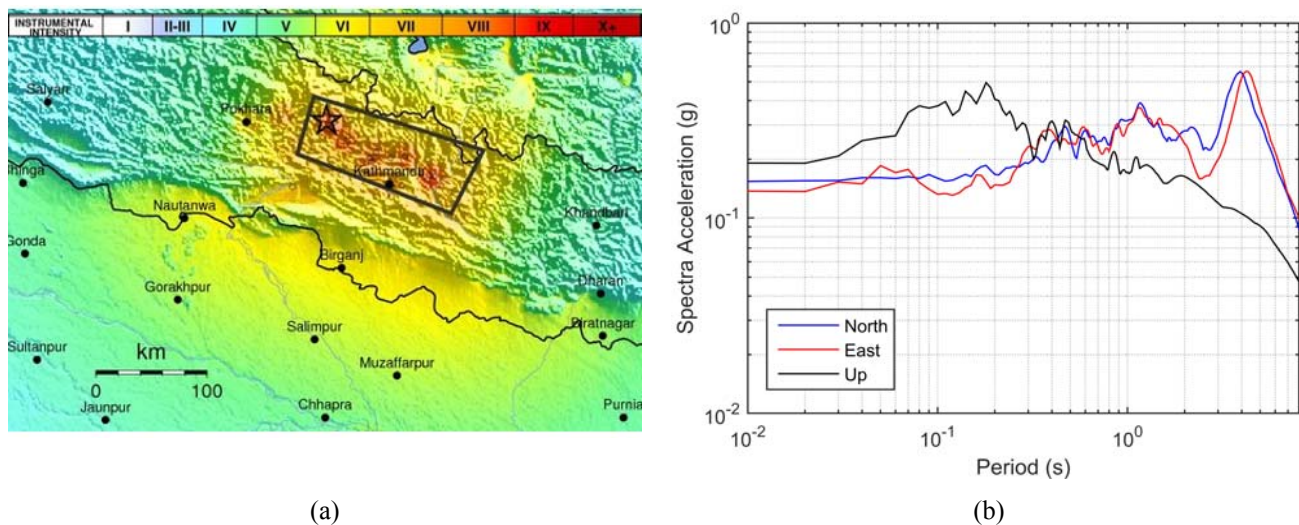


Fig. 1 – Details of the 2015 Gorkha earthquake (main shock): (a) Isoseismic map of estimated Modified Mercalli Intensity scale (I-X) [2] and (b) 5% damped critical spectral accelerations at the THM station west of Kathmandu (27.68130° N, 85.37705° E) [3].

The Himalayan Mountains are located at the collision of two continental plates, namely the Indian and Eurasia plate that contribute to the seismic risk of Nepal [4]. The 2015 Gorkha earthquake is the most severe earthquake in this region since the 1934 Nepal-Bihar earthquake [5], leading to widespread damage, loss of life throughout the country, and loss of irreplaceable cultural heritage. In this event, the estimated number of deaths and injuries was nearly 8,600 and 22,000, respectively. In addition, nearly 780,000 buildings were severely damaged and approximately 300,000 buildings were partially damaged [6]. Estimates of total rebuilding cost are more than \$10 billion USD, which equates to 50 percent of the Nepali GDP [7].

One heavily damaged historic village in the Kathmandu Valley was Bhaktapur. Bhaktapur is an 18th century Newar city in the eastern section of the valley, approximately 13 km from downtown Kathmandu. This city was the largest of the Newar kingdoms and home to the historic and iconic Nyatapola temple, which has been declared as UNESCO world heritage site. This temple is a five-story pagoda style unreinforced brick masonry with mud-mortar structure originally completed in 1702. It is currently the tallest temple in Nepal, although historically other tall temples are known to have been destroyed over time due to previous earthquakes in the region. This temple had previously survived the 1934 Nepal-Bihar earthquake and was fortunate to remain upright, even though the topmost roof of the temple was destroyed. During the 2015 event, this temple was heavily damaged as evidenced in large cracks opening in the masonry walls at the base level. Other temples were damaged in the 2015 Gorkha earthquake, including others in Bhaktapur and Durbar square (downtown

Kathmandu). On June 26, 2015, the authors visited this site to characterize its damage using ground-based light detection and ranging (lidar) and ambient vibrations. Lidar provides a geometric assessment of the current condition of the temple, indicating whether any post-earthquake drift exists as a function of height as well as if any significant cracks are present in the façade. Ambient vibrations, collected via accelerometers placed on various levels of the temple, permit an estimation of the vibrational properties via operational modal analysis. This study utilizes the frequency domain decomposition method to estimate the fundamental frequencies of the structure from three accelerometer setups using an output only approach. The response of the structure under earthquake loading not only depends on the structural system itself but also the soil and foundation parameters, location of structure, and nature of earthquake. Hence, the best knowledge available and gathered by the authors is presented herein.

2 Structural Details

The structural system of this five tiered pagoda temple develops around a shrine that sits at the base of the temple, immediately above the plinth (pedestal). The plinth (Fig. 2a) consists of elements that support the large stairway (of five levels) that provides access to the main temple entrance on the south wall. The plinth is 5 m tall. The main structure of the temple develops immediately above the plinth. In plan view, the temple is square. An unreinforced brick masonry with mud mortar core wall system develops in the middle, surrounding a 3.40 m x 3.40 m open space, where the shrine is housed. A walkway between outer timber columns surrounds the core wall at the base level. The walls are perforated at the base with door openings on each side. Along the height of the temple, the walls reduce in thickness. For the first and second story, the main core wall is 1.59 m thick, and have a height of 6.78 m and 4.54 m, respectively. In the first story, above the door openings, there are heavy timber cross-beams that support the load-bearing wall over a height of 3.66 m. In the third story, the wall thickness is reduced to 1.20 m, and the story develops over a height of 4.33 m. The change in wall thickness between stories is achieved by the use of heavy timber cross-beam load transfer elements. These timber elements aid in the formation of timber floors, which penetrate the walls and are tied to the roof structures. In stories 4 and 5, the wall thickness reduces to 0.99 m and 0.66 m, respectively, while the story heights are 3.02 m and 3.26 m, respectively. The total height of the temple is achieved with a central spire that is approximately 3.00 m tall that is attached approximately at two-thirds height of the walls in story 5.



(a)



(b)

Fig. 2 – View of the Nyatapola Temple: (a) overview of the entrance from the south plaza and (b) view of the north wall with significant shear cracks.

3 Field Survey and Data Collection

3.1 Lidar Data Collection

Ground-based light detection and ranging (lidar) technologies have evolved significantly in the last decade and have become more commonplace in engineering applications. Within structural engineering, lidar has been used to capture complex geometry, deformation, and damage to various structures because it is a highly accurate and detailed nondestructive evaluation technique [8-14]. As a result, it has a potential to become a prevalent method for structural health monitoring and condition assessment during routine inspections or following extreme events such as earthquakes [e.g., 15-17]. Lidar platforms can rapidly measure angles and distances to objects based on speed of light or the phase difference between the emitted and reflected laser beams (Fig. 3). The output from a lidar scanner is a point cloud, a quantifiable, three-dimensional, virtual model of objects within its field-of-view. In general, the accuracy within a lidar point cloud is a function of the equipment, scan setting, scan strategy, and local environment and will vary by each point. Nonetheless, local measurements within the point cloud can typically be made at the sub-centimeter level for small sites or structures.



Fig. 3 – Lidar scanning at Bhaktapur’s Nyatapola Temple: (a) Faro Focus^{3D} X 130 and (b) Riegl VZ-400 laser scanners.

During the site investigation of the Nyatapola Temple, the team conducted 38 ground-based lidar scans with two lidar scanning platforms: a Faro Focus^{3D} X 130 (Fig. 3a) and a Riegl VZ-400 (Fig. 3b). The Faro Focus^{3D} X 130 scanner has a 1550 nm wavelength laser and can capture up to 976,000 points per second up to a range of 130 m with a ranging error (1- σ) of ± 2 mm and a field of view of 360° horizontally, 300° vertically, and a minimum angular resolution of 0.009° [18]. Similarly, the second lidar scanner, Riegl VZ[®]-400, employs a near-infrared laser to acquire longer range data up to 350 m with an estimate ranging accuracy (1- σ) of 5 mm and a field of view of 360 ° degrees horizontally, 100° vertically, and a minimum angular resolution of 0.005° [19]. To optimize the data collected, the Riegl system scanned the structure from a longer distance at 13 different scan locations through a closed traversed scanning strategy to capture details of the structure at greater elevations as well as nearby buildings and topography (Fig. 4a). Static GNSS coordinates (processed against a base station located < 1km from the site) were also obtained for several of the scan positions to geo-reference the lidar data into UTM coordinates. The closed traversed scanning strategy reduced registration utilized paper checkerboard targets as well as cloud-to-cloud constraints for an average relative error of 7 mm (3D). In a complementary

manner, the Faro laser scanner collected detailed data on the tiered support structure and at the ground level of the temple within a meter of the exterior wall. Twenty-five Faro were conducted also in a closed traversed method with minimal occlusion (Fig. 4a). The point cloud was registered without targets (due to the inability to place targets on the historic structure) for an average registration error of 2 mm (3D) between overlapping scans. Then, to create a holistic scene of the temple, both lidar set (38 scans) were registered in a unified coordinate system using a cloud-to-cloud optimization (Fig. 4b). The average error the overall registration for the unified point cloud of both systems was 1 cm (3D) with a sampling distance of less than a centimeter at ground level.

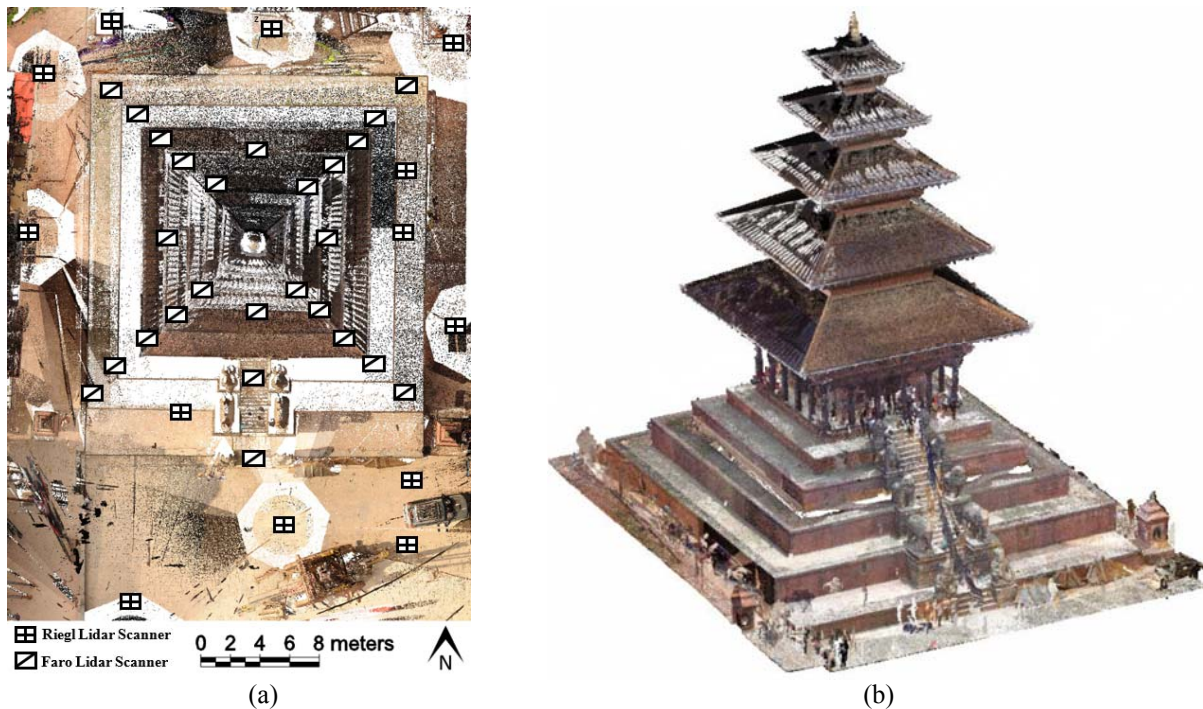


Fig. 4 –Point cloud view (a) top view of scan locations for both the Riegl and Faro lidar scanners and (b) isometric view of registered unified point cloud.

3.2 Ambient Vibration Data Collection

On June 26th, 2015 the authors collected lidar and ambient vibration recordings (Fig. 5). During the afternoon and evening hours, vibration recordings were obtained at this temple structure using 12 piezoelectric accelerometers operating at 2048 Hz in three different setups as shown Fig 6a. Note the excitation for this ambient vibration was primarily due to pedestrian traffic and low-to-moderate wind velocity structures. For each setup, the story level (accelerometer placed on the pagoda roof overhangs) varied while the base level positions were held constant. The first setup consisted of levels 6, 5, and the base; while the second setup consisted of levels 4, 3, and the base. Likewise, the third and final setup consisted of levels 2, 1, and the base. The base level, top level of the plinth, was kept constant to provide a reference measurement between each of the three setups. At each floor level, the accelerometers were placed at the central location of each free edge of the roof structure (Fig. 6b). However due to the historic and religious significance of this structure, the authors were not permitted to enter the temple. Therefore, the authors instructed local climbers to delicately place and attach the sensors at the desired location and direction, to the best of their ability. At each setup, the duration of the ambient recordings was 24 minutes. During initial field processing of the data, some of the channels were indicated as faulty, which may be attributed to the placement of the sensors, poor cabling, voltage spikes in the field, and accelerometer attachments. However, this concern will be discussed in section 5 in more detail.



Fig. 5 – Example instrumentation implemented in the field: portable data acquisition, accelerometers, and field laptop.

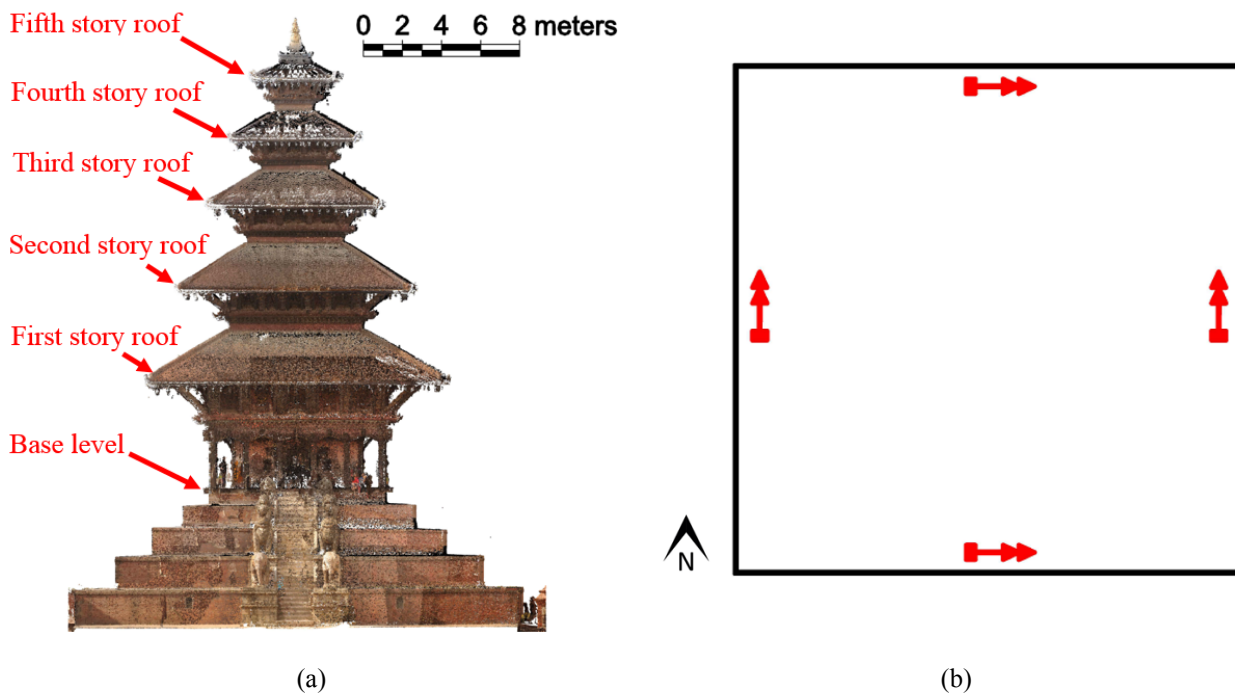


Fig. 6 – Instrumentation setups (a) overview of floor levels indicated on the point cloud (view from the south), (b) typical sensor placement on the face of each roof overhang.

4 Damage Characterization Using Lidar

4.1 Estimation of Global Torsional Deformation

The five-story Nyatapola temple structure comprises of a timber frame with brick masonry infill walls, mud mortar, and timber floors; contributing to its classification of a structure with of its flexible diaphragms. After the 2015 Gorkha earthquake, severe cracking and grout loss was noted on all interior and exterior walls at the ground level of the structure. The residual deformation of the unified point clouds confirmed these damaged patterns observed in the structure. To accomplish this task, six slices of the complete point cloud starting at the base level to the top level are exported and compared to the ground level to identify any residual torsional drift (Fig. 7). Estimated residual torsional drifts for the first to fourth stories are 0.00°, 0.19°, 0.65°, and 1.20° anticlockwise, respectively; while a significantly larger clockwise rotation of 3.82° is noted at the fifth floor. These residual torsional drift values can be attributed to the earthquake response of the temple (for the second

and fifth floors) as verified by the ambient vibrations. However, this assumes that the building was constructed perfectly rectangular, which is unlikely to be the case.

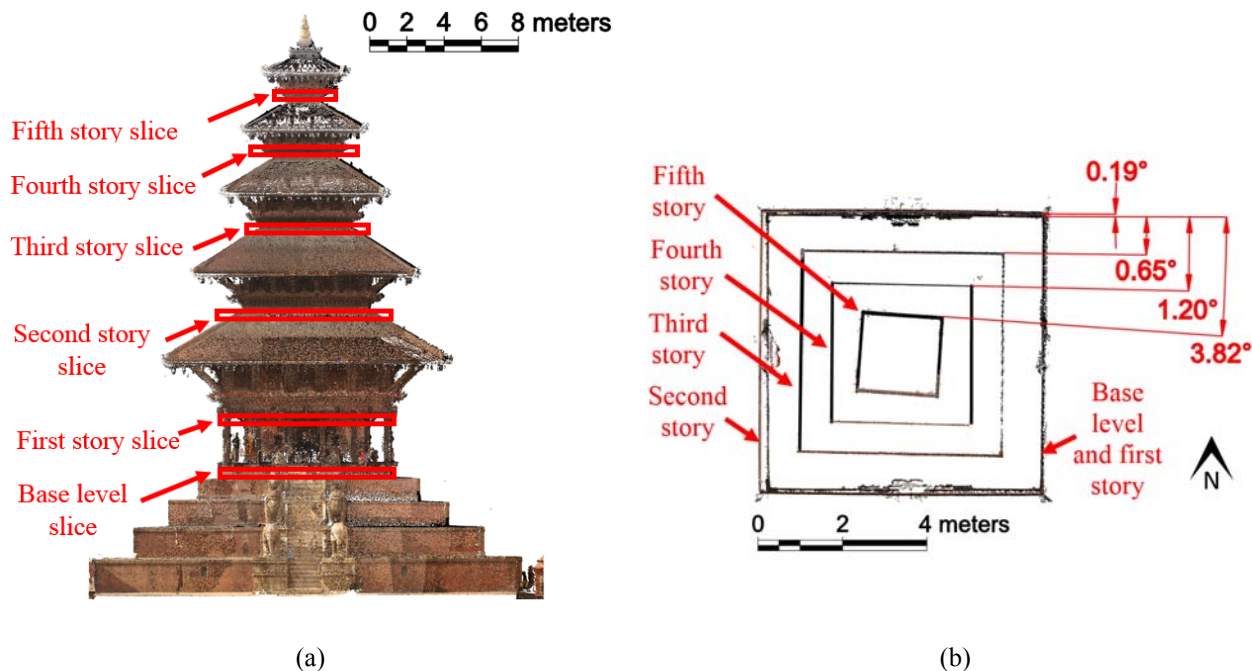


Fig. 7 – Estimation of torsional permanent drift: (a) elevation view highlight location of the point cloud slices and (b) torsional drift as estimated from these slides by story.

4.2 Identification of Locations with Maximum Damage

Quantification of the major cracks located within the first story masonry walls are identified from the twelve close-range (less than 1 meter) scans. The variation of the surface geometry can identify cracks and present detailed architectural features from the collected point cloud set [14]. In the first step, a distance-based weighted averaging method computes the normal vectors for each of the vertices based on five nearest neighbors. Afterward, the dot products of the normal vectors are computed with respect to best-fit reference plane for the entire point cloud set. Finally, through investigation of underlying distribution of the dot product results, surface defects are detected for those points which deviate most significantly from the best fit plane. Within each colorized point cloud, a red color indicates the vertices that were identified as a surface defect while undamaged points become as black colored vertices. Fig. 8a illustrates various surface defects such as a shear crack. However, note that this approach also detects architectural features (ornate wooden door and header).

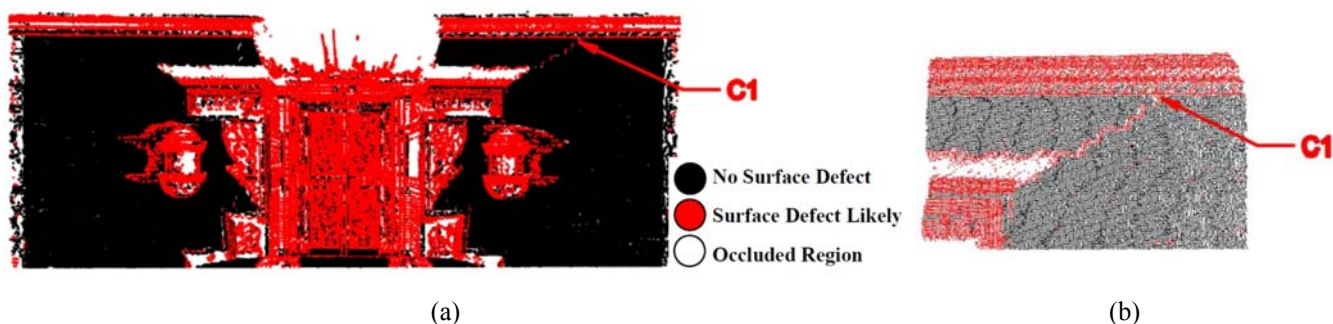


Fig. 8 – Crack locations identified at the ground level for the north exterior wall: (a) overview and (b) detailed view.

A detailed view of a significant shear crack (C1) is presented in Fig 8b. To quantify the defect, both length and the width of crack were measured as 1.27 m and 3.3 cm, respectively. Assuming that the crack consisted of a series of straight lines, the summation of the crack lengths can be directly computed. However, the width of the crack varies along its length; therefore, the average value of ten different width measurements is reported.

5 Damage Characterization Using Ambient Vibration

5.1 Introduction and Previous Study

Damage detection within structures is the common goal in structural health monitoring (SHM). Numerous nondestructive techniques have been employed for SHM such as impact echo, ground penetrating radar, and infrared imaging; however, these methods typically require time consuming, on-site investigations that may have cost and accessibility limitations. One method that addresses many of these shortcomings is damage detection using acceleration responses through system identification techniques of experimental or operational modal analysis. These algorithms provide an estimate of the dynamic and modal properties of the structure of interest system properties (e.g., frequency) [20]. Recently developed, low sensitivity accelerometers can detect small variations in vibrational responses if placed strategically within the structure even under normal operational loads or ambient vibrations. These system identification techniques permit an analyst to correlate the vibration response data to a mathematical model of the system (or a finite element model). Therefore, the verified models using the identified modal parameters can be used for further analytical studies with higher confidence [e.g., 21 and 22].

Jaishi et al. [23] performed seismic assessments of ten typical multi-tiered temples throughout Nepal using ambient vibration (operational modal analysis) and a parametric study of finite element models (FEM). The FEM models were manually tuned using the estimated modal parameters from ambient vibrational responses under wind and traffic excitations. The operational modal analysis was conducted using two methods, namely peak picking and stochastic subspace identification (SSI). In addition, this study developed an empirical formula that can estimate the natural periods of vibration of Nepali temples (undamaged) with approximately a 1.0 Hz error. Specifically for the Nyatapola temple, the first six natural frequencies identified via peak picking as 1.69 Hz (bending in the north-south direction), 1.71 Hz (bending in the east-west direction), 3.91 Hz (2nd mode bending in the east-west direction), 3.93 Hz (2nd mode bending in the north-south direction), as well as 5.1 Hz and 6.1 Hz as torsional modes. Note the 3.91 Hz and 3.93 Hz modes are closely spaced and may be indicative of the first torsional mode of the structure.

5.2 Identification of Natural Frequencies

In this preliminary assessment of the natural frequencies, only the third accelerometer setup was utilized. For this third setup, the three channels selected include 2S-E, 1N-E, and 1E-N. This nomenclature indicates that accelerometer 2S-E is placed on the south face of the 2nd level where the positive direction is defined as eastward. The remaining channels were not considered due to inherent noise likely from poor cable connections, wet cables and moisture on the structure, improper/loose attachment of the accelerometer to the structure, and voltage spikes of the power source. Due to the reduced channel count, frequencies are reported herein using an output only approach. Further studies may attempt to extract characteristic deflect shapes.

The acceleration time histories of each channel are filtered first for high voltage spikes using a Hampel identifier function of a neighborhood of five times the sampling rate (five seconds) and for values greater than five times the standard deviations from the neighborhood median. Then the channels are filtered in the frequency range of 1.1 Hz to 20 Hz using a Finite Impulse Response filter of order 8192. To estimate the natural frequencies, the 24-minute duration of acceleration data is divided into 30 divisions and the power spectral density computed. From the average power spectral density plots, the natural frequencies are extracted (as local maxima) as illustrated in Fig 9. Using the peak-peaking method, the first three excited modes are identified as 1.51 Hz, 2.55 Hz, and 3.31 Hz. Note all of these modes are identified as torsional (considering all three accelerometer setups), since modal coordinates have values in each direction of the structure at various levels. A frequency shift in the fundamental mode from 1.69 Hz to 1.51 Hz is observed when comparing the pre- and post-earthquake system

identification results. This shift represents a 16.8% period elongation in the structure, which is significant and demonstrated by the large shear cracking at the ground level (above the plinth). In the post-earthquake system identification, it is noted that the first four modes are torsional and may or may not be coupled with bending (currently inconclusive). The behavior is further confirmed in the temple assessment since the observed damage is not uniformly distributed and the greatest damage in terms of frequencies and crack widths is located at the north wall.

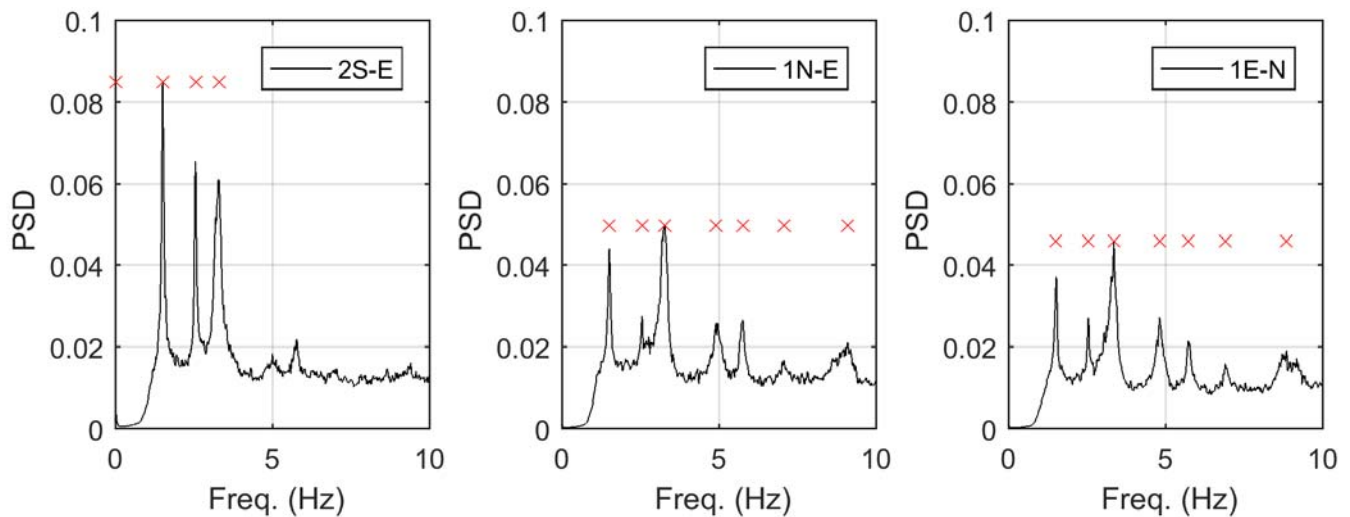


Fig. 9 – Identified modes by peak peaking following the 2015 Gorkha earthquake and its subsequent aftershocks.

5.3 Linear Finite Element Model

Finite element modeling (FEM) is a common methodology to further study the behavior and response of structures under complex loading. There are multiple levels of modeling to consider, however for this study the macro-level is considered. Finite element of masonry structures is not a trivial task due to the complexity of the masonry units, mortar, and their interaction. In this modeling approach, the load bearing walls are considered as structural elements, while struts and roof systems are considered nonstructural and only accounted for as gravity loads and assigned masses as manually estimated. The FEM is constructed within SAP2000 v18 and the temple walls are constructed using three-dimensional solid elements. The floor levels are currently considered as rigid, as the concentration of the timber joists is high. Additionally, boundary constraints are applied at the floor level joints to provide rigidity. The base of the structure is fixed, neglecting any soil-structure interaction as well as the dynamic response of the plinth. Initial material properties were also chosen based on the previous work and include a density and Young's modulus of 2000 kg/m³ and 800 MPa as well as 800 kg/m³ and 1.25 GPa for the mud-mortar brick masonry and timber elements, respectively. After the model was constructed in SAP2000 v18, an eigenvalue analysis was performed to illustrate the model's modal properties. The first four natural modes are identified and illustrated in Table 1 and Fig. 10.

To date, the model was constructed to closely resemble the work done by Jaishi et al. [23] for validation purposes. Further model refinement for this pre-earthquake state will be conducted in future work. Using the post-earthquake identified data and lidar detected crack patterns, linear finite element model updating will be conducted to closely resemble the current structural state (post-earthquake). This updated FEM will be useful in seismic vulnerability studies of this and other pagoda style temples as well as possible retrofitting schemes.

Table 1 – FEM identified modes for the pre-earthquake structural state (refer to Fig. 10).

Mode Shape No.	Frequency (Hz)	Period (s)	Note
Mode 1	2.100	0.476	Translation in YZ
Mode 2	2.101	0.475	Translation in XZ
Mode 3	5.448	0.183	Torsion about Z
Mode 4	6.281	0.159	Translation in YZ and XZ

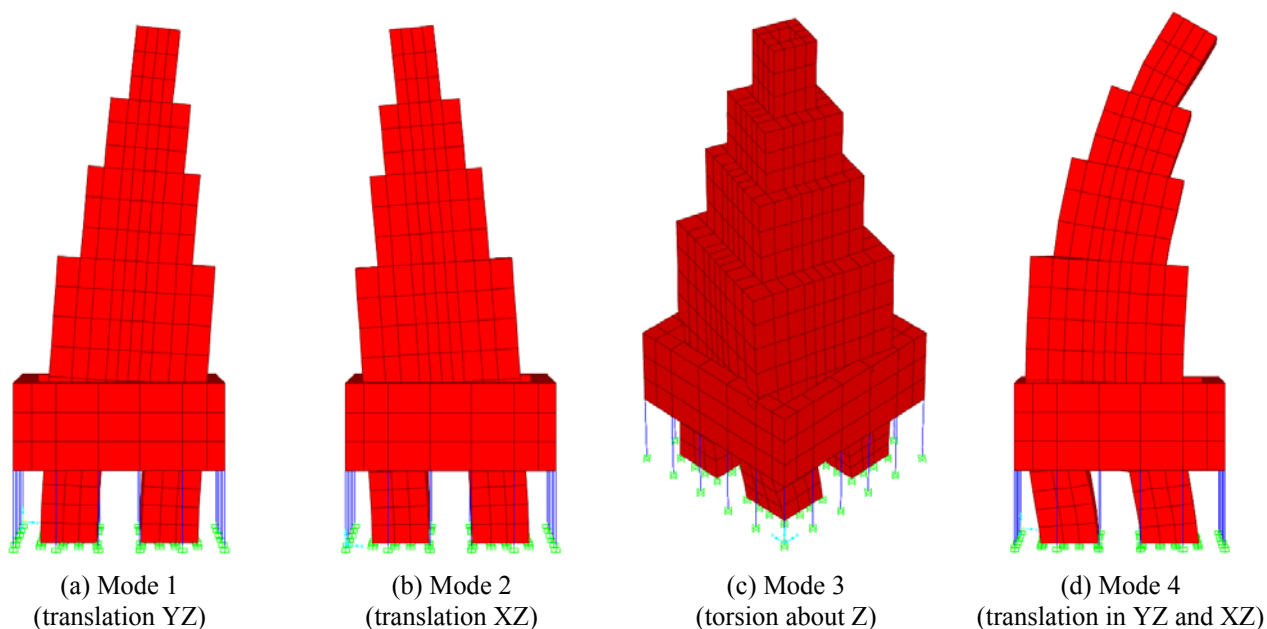


Fig. 10 – First four fundamental models for the linear FE model performed in SAP2000 v18.

6 Conclusions

This paper studies the preliminary damage detection and system identification of the Nyatapola Temple following the 2015 Gorkha earthquake and its subsequent aftershocks. This five-story pagoda style temple was severely damaged in non-uniformly distributed pattern due to torsion. Lidar and ambient vibrations characterized its current structural condition. Lidar data quantified an observable torsional permanent drift of all story levels except one, where a 3.8° clockwise rotation was estimated at the top level. Note this observed torsional response was also noted in the observable damage at the base level, where cracks greater than 3.0 centimeters in width were found. Lidar data also produced a digital survey of detected surface defects through a localization and quantification of cracks, where the north wall was found to be most severely damaged. To confirm these observations, output-only system identification of the ambient responses provided estimates of the excited post-earthquake natural modes in a torsional response. In comparison of the fundamental mode via peak-peaking methods, the post-earthquake fundamental frequency shortened from 1.69 Hz to 1.51 Hz for a percent difference of 16.8%. This significant period elongation (or frequency shortening) highlights the current vulnerability of this structure for future seismic events. Future work includes linear finite element model updating for the post-earthquake condition to investigate this temple's seismic vulnerability as well as possible retrofitting schemes.

7 Acknowledgements

Support for this work was provided by the University of Nebraska Foundation and NSF CMMI Award #1545632 at Oregon State University. In conducting this fieldwork and data processing, the authors would like to greatly acknowledge the support from Mr. Supratik Bose of the University at Buffalo as well as numerous individuals at Oregon State University (OSU) including Prof. Dan Gillins, Mr. Patrick Burns, Mr. Matthew Gillins, Mr. Rajendra Soti, and Mr. Matthew O'Banion. Site access was graciously provided by Bhaktapur Municipality in coordination with Khwopa College of Engineering. Accelerometer equipment was generously provided by Prof. Babak Moaveni of Tufts University. Additionally, the authors also acknowledge the support of Leica Geosystems as well as David Evans and Associates for providing equipment and software utilized in this study at OSU. The opinions expressed in this paper are those of the authors and do not necessarily represent those of the sponsors or the collaborators.

8 References

- [1] Rai DC, Singhal V, Raj SB, Sagar SL (2015): Reconnaissance of the effects of the M7. 8 Gorkha (Nepal) earthquake of April 25, 2015. *Geomat. Nat. Haz. Risk*, **7** (1), 1-17.
- [2] United State Geological Survey (2015): M7.8 – 36km E of Khudi, Nepal. http://earthquake.usgs.gov/earthquakes/eventpage/us20002926#general_region. (Feb. 19, 2016).
- [3] Takai N, Shigefuji M, Rajaure S, Bijukchhen, S, Ichiyanagi M, Dhital MR, Sasatani, T (2016): Strong ground motion in the Kathmandu Valley during the 2015 Gorkha, Nepal, earthquake. *Earth, Planets and Space*, **68** (1), 1.
- [4] Paudyal H, Panthi A (2010): Seismic Vulnerability in the Himalayan Region. *Himalayan Phys.*, **B** (1), 14-17.
- [5] Hashash Y, Tiwari B, Moss RE, Asimaki D, Clahan KB, Kieffer DS, Dreger DS, Macdonald A, Madugo CM, Mason H B (2015): Geotechnical Field Reconnaissance: Gorkha (Nepal) Earthquake of April 25, 2015 and related shaking sequence. *Geotechnical Extreme Event Reconnaissance GEER Association Report no. GEER-040*, San Luis Obispo, CA, USA.
- [6] Nepal Disaster Risk Reduction Portal (2016): Incident report of earthquake 2015. <http://drrportal.gov.np/>, (Feb. 19, 2016).
- [7] Bloomberg (2015): Nepal says earthquake rebuilding cost to exceed \$10 billion. <http://www.bloomberg.com/news/articles/2015-04-28/nepal-rebuilding-cost-to-exceed-10-billion-finance-chief-says>, (May 13, 2016).
- [8] Kayen R, Olsen MJ (2012): Post-earthquake and tsunami 3D laser scanning forensic investigations. *J. Forensic Eng.*, 2012: pp.477-486.
- [9] Olsen MJ (2013). In situ change analysis and monitoring through terrestrial laser Scanning. *J. Comput. Civ. Eng.*, **29**(2), 04014040.
- [10] Mosalam KM, Takhirov SM, Park, S (2014): Applications of laser scanning to structures in laboratory tests and field surveys. *Struct. Control Hlth.*, **21** (1), 115-134.
- [11] Wood RL (2014): Methods of structural damage characterization for infrastructure. *34th Annual Structural Congress*, Structural Engineering Association of Nebraska, Omaha, NE, USA, 12pp.
- [12] Wittich CE, Hutchinson TC, Wood RL, Seracini M, Kuester F (2015): Characterization of full-scale, human-form, culturally important statues: case study. *J. Comput. Civ. Eng.*, 05015001.
- [13] Wood RL, Mohammadi ME (2015): LiDAR scanning with supplementary UAV captured images for structural inspection. *International LiDAR Mapping Forum*, Denver, CO., USA.
- [14] Mohammadi ME, Yousefianmoghadam S, Wood RL, Stavridis A (2016): Damage quantification from point clouds for finite element model calibration. *SEI/ASCE Structural Health Monitoring Applications Case Study Archive*.
- [15] Olsen MJ, Cheung KF, Yamazaki Y, Butcher S, Garlock M, Yim S, McGarity S, Robertson I, Burgos L, Young YL (2012): Damage assessment of the 2010 Chile earthquake and tsunami using terrestrial laser scanning. *Earthq. Spectra*, **28** (1), 179-197.

- [16] Kashani A, Olsen MJ, Graettinger A (2015): laser scanning intensity analysis for automated building wind damage detection. *Proceedings of International Workshop on Computing in Civil Engineering*, Austin, TX, USA, 21-23.
- [17] Bose S, Nozari A, Mohammadi ME, Stavridis A, Moaveni B, Wood RL, Gillins D, Barbosa A (2016): Structural assessment of a school building in Sankhu, Nepal damaged due to torsional response during the 2015 Gorkha earthquake. *IMAC XXXIV A Conference and Exposition on Structural Dynamics*, Orlando, FL, USA, 25-28.
- [18] Faro (2011): Faro laser scanner Focus 3D: features, benefits & technical specifications. FARO Technologies, Lake Mary, FL, USA.
- [19] Riegl (2014): Riegl VZ-400 datasheet, Riegl Laser Measuring Systems GmbH, Austria.
- [20] Doebling SW, Farrar CR, Prime MB, Shevitz DW (1996): *Damage identification and health monitoring of structural and mechanical systems from changes in their vibration characteristics: a literature review*. No. LA--13070-MS, Los Alamos National Lab, NM, USA.
- [21] Michel C, Guéguen P, Bard P (2008): Dynamic parameters of structures extracted from ambient vibration measurements: An aid for the seismic vulnerability assessment of existing buildings in moderate seismic hazard regions. *Soil Dyn. Earthquake Eng.*, **28**(8), 593-604.
- [22] Shahidi SG, Pakzad SN, Ricles JM, Martin JR, Olgun, CG, Godfrey EA (2015): Behavior and damage of the Washington Monument during the 2011 Mineral, Virginia, earthquake. *Geol. Soc. Spec. Pap.*, 509 235-252.
- [23] Jaishi B, Ren W, Zong Z, Maskey PN (2003): Dynamic and seismic performance of old multi-tiered temples in Nepal. *Eng.Struct.*, **25** (14), 1827-1839.